Experimental measurements of the nonlinear Rayleigh-Taylor instability using a magnetorheological fluid

Jeremy White, Jason Oakley, Mark Anderson, and Riccardo Bonazza
Department of Engineering Physics, University of Wisconsin–Madison, Madison, Wisconsin 53706, USA
(Received 21 November 2008; revised manuscript received 21 August 2009; published 8 February 2010)

The unique properties of magnetic fluids are exploited to create a static interface between two fluids in the context of studying Rayleigh-Taylor (RT) driven mixing. Paramagnetic fluids have previously been used for studying this phenomenon [Z. Huang *et al.*, Phys. Rev. Lett. **99**, 204502 (2007)], as have ferrofluids [G. Pacitto *et al.*, Phys. Rev. E **62**, 7941 (2000)], but we propose using magnetorheological fluids instead to attain better control of the initial condition. As the motivation for using this technique is to quantify the effects of the initial condition on late time behavior of the RT instability, it is important that the initial condition be prescribed at a scale large enough to reliably measure. As a first demonstration of creating such an interface, this technique is applied to the two-dimensional (2D) instability with a single-mode sinusoidal interface. This technique has been used to study both moderate and high Atwood number systems, with successful control of the interface in an $A=1$ system being demonstrated. The nonlinear growth phase for this initial condition is examined and comparisons are made with both analytical models and published numerical and experimental work on the 2D single-mode RT instability. Measurements of the late time RT spike behavior reveal poor agreement between the experimental results and the analytical models.

DOI: 10.1103/PhysRevE.81.026303 PACS number(s): 47.20.Ma, 47.65.Cb

When two fluids of different densities, separated by a perturbed interface, are accelerated normal to the interface, vorticity is baroclinically generated by the misalignment of the density and pressure gradients. This vorticity generation leads to the unbounded growth of the interfacial perturbations known as the Rayleigh-Taylor (RT) instability [1–3]. This instability plays a significant role at very large scales in the case of a supernova, and at the very small scales present in inertial confinement fusion, where fluid mixing consequent to the interface distortion and breakup is detrimental to the energy output from the reaction.

The growth of these perturbations and the mixing process in general can be broken up into four different and distinct flow regimes. In the linear regime the amplitude is still much smaller than the wavelength and the different modes of the perturbation grow independently of one another, exponentially in time [3]. Deviations from this exponential growth begin to occur when the amplitude of the perturbations grows to $\sim 0.1\lambda - 0.4\lambda$ [4], after which the amplitude growth saturates for single-mode interfaces and then evolves into a state of self-similar mixing for multimode initial conditions. It is these later stages of the progression of this instability, where amplitude growth saturation and self-similar mixing occur, that are the focus of most current investigations since the early time behavior is well characterized by Taylor's linear theory which has been validated by experiments and simulations. However, there is less consistency between theory, experiments, and simulations for the nonlinear growth regime where the transition to saturation occurs. One of the biggest challenges with the experimental work is the difficulty in prescribing and characterizing the initial condition. Concerning single-mode perturbations, the most common method of generating the initial condition involves agitating the interface of an initially stable stratification. The original experiments performed by Lewis to validate Taylor's theory used an oscillating paddle to disturb the interface [4]. A similar perturbation technique is employed by Emmons *et al.* [5]. Later work improved upon these experiments by oscillating the tank containing the liquids to produce a standing wave on the interface [6–8]. Each of these experiments began with an initially stable fluid stratification and uses an acceleration mechanism to drive the instability.

There are also techniques utilizing gravitational acceleration of an initially unstable stratification. While these methods [9–11] eliminate the complications from artificial acceleration, they do give rise to other issues regarding control of the initial perturbations and precise knowledge of those initial conditions. A more recent technique is to make use of the unique properties of magnetic liquids. As demonstrated by Huang *et al.* [12], such fluids can be used to create an initially unstable stratification without the use of a plate for separation or any need to invert the test section. Although control of the wavelength of the perturbations has been demonstrated, one possible outstanding issue with these experiments is the inability to directly measure the initial conditions as a result of the extremely small amplitudes. In another set of experiments utilizing magnetic fluids, the control of the perturbations relied upon forcing a magnetic instability of the particular fluid used [13].

In this paper, we demonstrate a technique designed to address many of the concerns arising from the previous experiments. This technique also makes use of magnetic fluids; however, we employ a different class of magnetic liquids than those used in the previous works [12,13]. One property exhibited by all magnetic liquids is the body force that is generated in the presence of a magnetic field can be used to suspend the magnetic fluid over a less dense fluid. The particular type of fluid used in these experiments is called a magnetorheological (MR) fluid. An additional property unique to this class of magnetic fluids is the state change that occurs in the presence of the magnetic field. The viscosity of an MR fluid increases rapidly with the strength of the applied

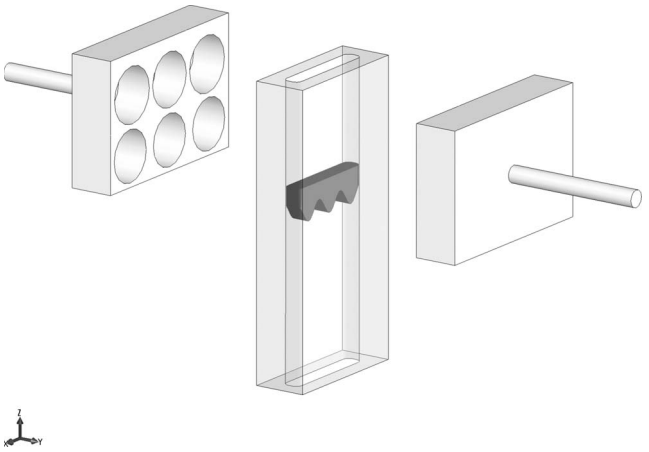

FIG. 1. Schematic of test cell with magnetic immobilization system.

field, to the point where the MR fluid behaves like a viscoplastic solid. This property facilitates good control of both the amplitude and wavelength of the initial perturbations as will be demonstrated. These fluids do have a finite reaction time to the magnetic field due to the formation and release of the fine structure that facilitates the viscosity changes. To the authors' knowledge this response time has not been experimentally measured. Instead, this time is referenced indirectly through the measurements of MR fluid device performance (such as shock absorbers), whose response times are on the order of 10 ms [14]. A very brief study was carried out in a past iteration of this experiment, based on varying the rate of removal of the magnetic field, to gauge any effect this fluid reaction time might have on the experiment and none was found.

Magnetorheological fluids can be created from a variety of different components differing based on the needs of the application; however, the same types of components are used in all mixtures. The fundamental ingredient in all MR fluids is carbonyl iron powder, comprised of spherical particles, usually 0.1–10 μm in diameter. The iron powder used in these experiments is the carbonyl iron powder CR from BASF, with particles having a mean diameter of 4.5 μm. This particular grade is selected for its optimal response to magnetic fields [15]. These particles are suspended in hexane with a volume fraction of particles $\phi=0.31$. A small amount ($\phi<0.005$) of the surfactant oleic acid is also added to prevent particle agglomeration. This formulation results in a MR fluid having a density of 2735 kg/m^3 and a viscosity of $\sim 5\times 10^{-3}$ Pa s. Coupling this fluid with water to form an interface results in an Atwood number of $A=(\rho_1-\rho_2)/(\rho_1+\rho_2)=0.46$. The MR fluid and water are immiscible and the interfacial tension between the two is estimated to be that between pure hexane and water, which is $\sigma=0.051$ N/m. Additionally, an interface is also set up using the same MR fluid and air resulting in an Atwood number of $0.999\sim 1$.

A simple procedure is used to set up the initial conditions with the MR fluid statically suspended over water. To create the shaped interface, an aluminum plunger with the desired perturbation machined into it is inserted into the test cell. Water is then poured over the plunger and frozen, thus taking the shape of the plunger. Once the plunger is removed, the MR fluid is poured over the ice. Next, the MR fluid is immobilized by placing the test cell between two banks of magnets, and the ice is then melted resulting in an interface between MR fluid and water. For the high Atwood number configuration, the water is drained leaving an interface between MR fluid and air. It is necessary to use ice for this process, as direct shaping of the MR fluid inside the magnetic field causes severe distortion of the interface shape. The magnet banks are attached to pneumatic cylinders that, when fired, retract from the test cell and release the immobilized MR fluid, thus allowing the instability to develop. A schematic of this setup is shown in Fig. 1. It should be noted that this pneumatic retraction system is completely divorced from the test cell so as to avoid any unwanted jitter during the retraction process. The test cell containing the fluids has an interior width of 7.6 cm, a depth of 1.27 cm, and a height of 22 cm. The side panels of the test cell are constructed of polyacetal with a thickness of $\sim$1.5 cm, while the front and back panels for viewing are made of acrylic with a thickness of 1.27 cm each. The banks of magnets shown are designed to create a relatively uniform field across the width of the test cell, with a positive gradient in the vertical direction. This is done using two rows of disk magnets with the top row containing stronger magnets. The state change of the MR fluid is due to the formation of chainlike structures which align themselves along the magnetic-field lines. This magnetically generated structure is what allows the fluid to keep its shape when the ice is removed eliminating the need for any further modulation of the magnetic field.

The diagnostics for this experiment present a particular challenge. Even very thin films of the MR fluid are optically opaque, and such films are deposited along the walls by the Rayleigh-Taylor spikes which can hide the vortex cores that

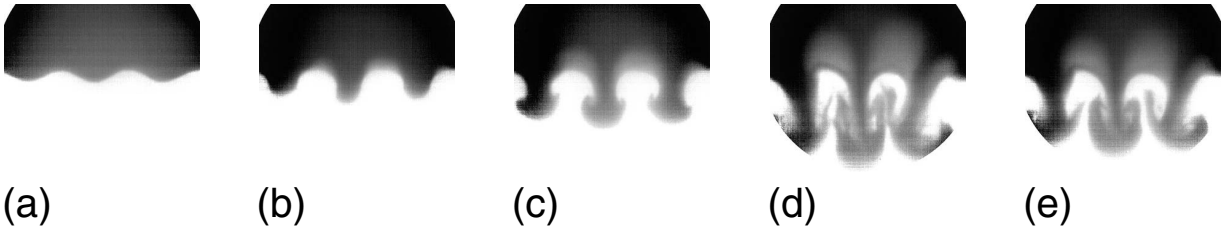

FIG. 2. Images from a typical $A=0.46$ experiment involving MR fluid (black) and water (white) showing the development of the instability from the initial condition to the late time nonlinear regime where the bubble and spike velocities have saturated. τ is a nondimensional time using a characteristic time $t'=\sqrt{\lambda/(Ag)}=0.068$. (a) $t=0$ ms, $\tau=0$ (b) $t=52$ ms, $\tau=0.74$ (c) $t=92$ ms, $\tau=1.31$ (d) $t=124$ ms, $\tau=1.77$ (e) $t=168$ ms, $\tau=2.4$.

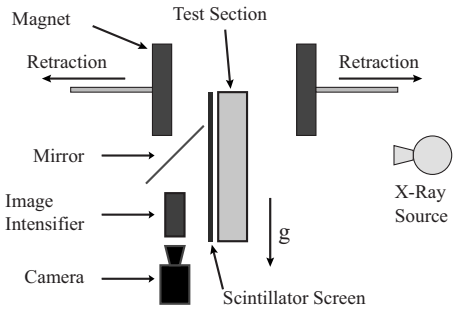

FIG. 3. Side view schematic of the experimental apparatus.

typically travel with the spikes. Further, as there is MR fluid in contact with the walls initially, there is also a film left on the walls as the RT bubbles grow which obscures the bubbles when using conventional backlight photography. To overcome this limitation, a high speed radiography system is employed. A continuous x-ray source operating at 110 kVp and 165 mA is used for a duration of 0.5 s for each experiment. The attenuated photons transmitted through the test cell are converted to visible light using a Kodak Lanex Regular scintillator screen. This screen is imaged using an image intensifier coupled to a Photron Ultima 1024 16k 1024 $\times 1024$ pixel CMOS camera recording at 250 frames per second. A sequence of five images taken with this imaging system for the $A=0.46$ configuration is shown in Fig. 2, while the physical layout of the equipment is shown in the schematic in Fig. 3. The second image sequence shows the development of the $A\sim 1$ configuration, Fig. 4. The moderate Atwood number setup shows the characteristic mushroom shapes associated with the RT instability, which are the result of shear-induced roll ups starting near the leading edge of the spikes due to the flow of water rising into the bubbles. No such roll ups are seen in the high Atwood number series as this shear-induced vorticity is not strong enough to entrain any of the lighter fluid due both to the reduced shear from the much lower viscosity of the lighter fluid and the very large inertia difference between the two fluids resisting the tendency of that shear to generate the roll up structure. The spikes do appear to narrow as expected, but only slightly before the leading edges grow beyond the boundaries of the interrogation window.

A wide range of initial conditions can be created by the technique described above; however, only a single-mode sinusoidal wave form is reported here to demonstrate the technique. This wave form has a wavelength of 2.12 cm and initial amplitude of 0.16 cm. A modal decomposition of the initial conditioin of a typical experiment via the Fast Fourier Transform is shown in Fig. 5, revealing the amount of control afforded by this technique. The large initial amplitude to wavelength ratio of the initial condition is on the verge of the transition to the nonlinear growth stage of the instability, which results in the departure from the linear theory at a very early time as shown in Fig. 6. The data presented in Fig. 6 represent 15 measurements and the error bars show the standard deviation at each point in time. The time axis is made nondimensional using a characteristic time for the system, $t'=\sqrt{\lambda/(Ag)}$ [16]. This definition appears to be a good marker of the transition to saturation of the velocity of the bubbles and spikes, as the growth rate appears to saturate at $t/t'\sim 1$. The experiments presented here extend only into the nonlinear regime where amplitude growth saturation occurs, prior to the start of the self-similar mixing regime.

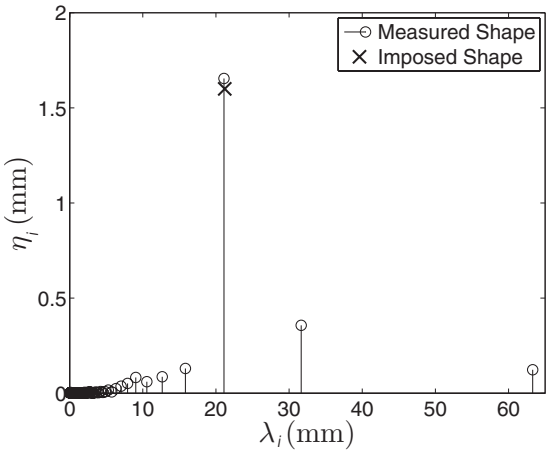

FIG. 5. Modal decomposition of the measured wave form compared with the imposed wave form.

There is a consensus that the velocities of the single-mode RT bubbles and spikes saturate at late times for $A<1$. This relationship is confirmed by measurements of the growth rate at late times, i.e., $t>t'$, the results of which are listed in Table I. These values are obtained by performing linear least-squares fits to the amplitude time history data from Fig. 6, where a linear relationship most closely matches the data. Significant asymmetry of the growth rates is observed between the bubbles and spikes. This is expected at moderate

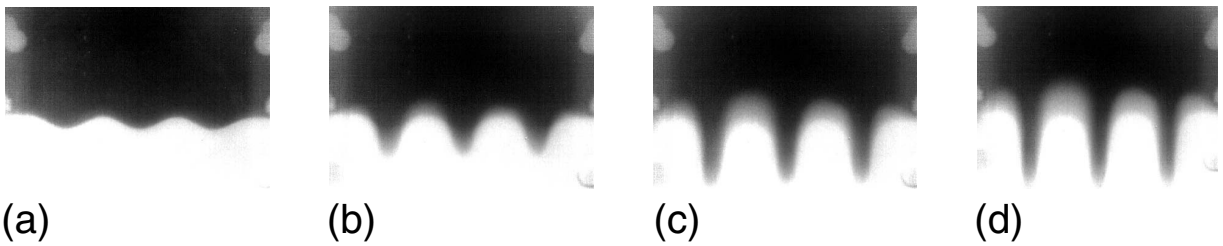

FIG. 4. Images from a typical $A=1$ experiment showing the development of the instability at an interface between the MR fluid (black) and air (white). In this configuration, only the velocities of the bubbles reach saturation while the spikes show continued acceleration before extending beyond the interrogation window. The characteristic time is $t'=0.047$. (a) $t=0$ ms, $\tau=0$ (b) $t=47$ ms, $\tau=1.0$ (c) $t=70$ ms, $\tau=1.5$ (d) $t=81$ ms, $\tau=1.75$.

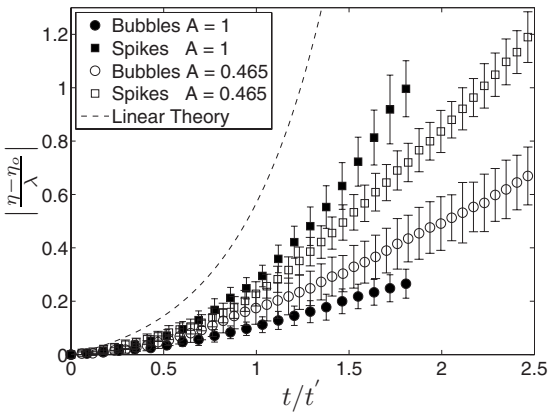

FIG. 6. Experimentally measured bubble and spike amplitudes as a function of time.

to high Atwood numbers, though the values do not agree well with the established (and frequently cited) nonlinear models of Oron *et al.* [17] and Goncharov [16]. These two models yield the same predicted values of the saturation velocities for the bubbles and spikes, given as $U_{b,s} = \sqrt{2Ag/[3(1 \pm A)k]}$ for the two-dimensional (2D) case, where (+) is for bubbles and (−) is for spikes. The two models are developed from different methodologies: a simple buoyancy-drag model in the case of Oron *et al.* and a potential theory formulation by Goncharov. It would seem reassuring that the two independently developed models achieve the same results, but comparisons with these experiments do not appear to support the accuracy of the models, especially with respect to the behavior of the spikes. Although the model does predict asymmetry in the saturated growth rates, the rates for the spikes are significantly less than the experimentally measured values as shown in Table I. This paper is not the first to show disagreement with these models; their accuracy is called into question in several recently published works [8,18,19]. Evidence of the deficiencies of the model are described by Goncharov [16] who shows a comparison of the 2D model and simulations at moderate Atwood numbers: the results for the bubbles compare favorably, while the spikes in the simulations greatly out pace the model. Similarly, Sohn [20] shows the same type of divergence with increasing Atwood numbers as compared with a slightly different potential theory model. Discrepancies such as those seen here for 2D are also observed in 3D when compared with both experiments [8] and numerical simulations [18]. Furthermore, a recent paper by Mikaelian [19] goes into detail to examine the limitations of the Layzer-type potential theory models. The guidance given for applying these models to the RT bubbles recommends an upper limit on the initial amplitude based on the wavelength and Atwood number, and this condition is satisfied by the initial conditions specified in these experiments, which is further evidenced by the relatively good agreement between the experiments and the model. Again, the use of the arbitrary Atwood number model for the RT spikes is not recommended, which is reflected in the poor agreement between these experiments and the model. It is worth noting when considering these results that these models do not incorporate the effects of the vortices (vortex pairs in 2D and vortex rings in 3D) near the head of the spike, viscous effects, or surface tension, all of which may contribute to the observed discrepancies.

TABLE I. Nonlinear growth rates: $\eta_o/\lambda = 0.07$.

		Experimental	Oron *et al.*
	A	U_∞ (mm/s)	$U_{\infty-2D}$ (mm/s)
Bubbles	0.46	106 ± 12	84
	0.99	94 ± 10	105
Spikes	0.46	209 ± 10	139

TABLE II. Late time acceleration measurements of the RT spikes for the $A=1$ configuration. Three nondimensional cutoff times are used to estimate the acceleration at successively later times.

		$(\frac{dU}{dt})_\infty$ (mm/s^2)
Exp.	$t/t' \geq 1.0$	6330
	$t/t' \geq 1.2$	6390
	$t/t' \geq 1.4$	6440
Zhang [21]		9807

It is clear from Fig. 6 that the rate of change of the amplitude of the spikes in the $A=1$ system is not saturating at late times. This is in agreement with the Layzer-type potential theory models: e.g., the model of Zhang [21] predicts an asymptotic acceleration for the spikes instead of an asymptotic velocity. A direct comparison of the experimental acceleration to this model is presented in Table II. There are three different values presented for the experimental results, with the nonlinear data truncated at successively larger nondimensional times. The largest measured accelerations are ~35% lower than the predicted free fall acceleration; however, the measurements indicate this acceleration to be continuing to grow. Unfortunately, as the spikes grow beyond the viewing window so quickly, the extent of this acceleration is unknown, so it is not certain how much higher the measured values of the acceleration would grow before saturating. There are also other effects which may be responsible for the discrepancy between the measurements and the model values. The model does not account for either surface tension or viscosity, both of which certainly have an effect on the flow in the experiments, especially surface tension as the two fluids are immiscible. These two factors serve to slow the progress of the spike down via viscous drag and by limiting how thin the spikes may become preventing the ideal asymptotic limit of an infinitely thin spike.

It is also important to look at how these results fit into the larger body of published results from other experiments and simulations. Complicating this task is the fact that these prior works all have different Atwood numbers and initial conditions making any direct comparisons difficult. One way to facilitate the comparison is to restate the results in another form such as the dimensionless Froude number. Taking the definition used in [8,18] gives Froude numbers of $\mathrm{Fr}_{b,s}$

TABLE III. Fr number comparisons for 2D single-mode studies.

Investigation	A	Fr_b	Fr_s	Fr_{avg}
Present experiments	0.46	0.37 ± 0.05	0.48 ± 0.01	0.43 ± 0.02
	0.99	0.29 ± 0.03	N/A	N/A
Analytical models [16,17]	0–1	0.325	0.325	0.325
Huang *et al.* [12]	0.29	N/A	0.52	N/A
Waddell *et al.* [7]	0.155, 0.336	N/A	N/A	0.306
Sohn [20]	0.05	0.311	0.313	0.312
Simulations	0.3	0.315	0.329	0.323
Ratafia [6]	0.095	~0.28	~0.28	~0.28

$= U_{b,s}/\sqrt{Ag\lambda/(1 \pm A)}$. The Froude numbers measured in these experiments as well as those predicted by the models are shown in Table III along with values from some other experiments and simulations of the 2D single-mode instability. Unfortunately, the body of work cited here does not provide a consensus as to what the Froude number should be. Results from both experiments and simulations seem to straddle the value suggested by the analytical models. There are some interesting points to take away from this information. First, the results from the experiments presented here and the results of the simulations of Sohn [20] both show an asymmetry in the measured values, with the spikes giving higher Froude numbers than the bubbles. The experimental results of Ratafia [6], however, do not appear to show any asymmetries at all, similarly to the models of Goncharov and Oron *et al.* The very low Atwood number in that study [6] is likely the reason for this, as no asymmetry is expected in that regime. Furthermore, the very low Atwood number results of Sohn [20] also show little asymmetry. These two studies point out that the models do appear to work well in the low Atwood number regime. Regrettably, no information on the asymmetry (or lack thereof) is reported in the works by Huang *et al.* [12] and Waddell *et al.* [7]. A positive result is that the relatively higher value of the Froude number in the present experiments as compared with the models is also seen in the reported results for the spikes in the experiments of Huang *et al.* As to the symmetry of the model values, this is expected as this Froude number definition uses the same characteristic velocity as the saturated velocity expressions given by the drag-buoyancy and potential flow models. The present experimental results for the bubble Froude number at the two Atwood numbers studied here straddle the model estimates just as with the measured saturated velocities. This may be due to periodicity issues as evidenced by the differing number of bubbles in each Atwood number configuration with the $A \sim 1$ experiments producing four bubbles while the $A = 0.46$ experiments routinely only showed two bubbles with large growth as shown in Figs. 2 and 4.

In summary, we have demonstrated the viability of using magnetorheological fluids to create a well-defined static interface between a MR fluid and another fluid for the purpose of studying the Rayleigh-Taylor instability. The demonstration of the technique was done with a simple periodic sinusoidal interface shape, and the experimental results reveal disagreements with the analytical models similar to those reported in some of the previous works, providing more evidence that these well established models may need to be reexamined particularly in the moderate Atwood number regime. The unique capabilities of this experimental technique are currently being used to examine the role of the initial conditions on the nonlinear behavior. Other more complex initial conditions will be studied, including continuous and discontinuous wave forms and single and multimode wave forms, with arbitrarily and independently variable amplitudes and wavelengths. Furthermore, extensions to multimode initial conditions will be utilized to examine the turbulent mixing regime and the associated models, again taking advantage of the interface shaping ability to gain a better understanding of the role of initial conditions in the development of the Rayleigh-Taylor instability.

[1] L. Rayleigh, Proc. London Math. Soc. **s1–14**, 170 (1882).
[2] G. I. Taylor, Proc. R. Soc. London, Ser. A **201**, 192 (1950).
[3] S. Chandrasekhar, *Hydrodynamic and Hydromagnetic Instability* (Clarendon Press, Oxford, 1961).
[4] D. J. Lewis, Proc. R. Soc. London, Ser. A **202**, 81 (1950).
[5] H. W. Emmons, C. T. Chang, and B. C. Watson, J. Fluid Mech. **7**, 177 (1960).
[6] M. Ratafia, Phys. Fluids **16**, 1207 (1973).
[7] J. T. Waddell, C. E. Niederhaus, and J. W. Jacobs, Phys. Fluids **13**, 1263 (2001).
[8] J. P. Wilkinson and J. W. Jacobs, Phys. Fluids **19**, 124102 (2007).
[9] M. J. Andrews and D. B. Spalding, Phys. Fluids A **2**, 922 (1990).
[10] P. F. Linden, J. M. Redondo, and D. L. Young,Phys. Fluids A **3**, 1269 (1991).
[11] S. B. Dalziel, P. F. Linden, and D. L. Youngs, J. Fluid Mech. **265**, 97 (1994).
[12] Z. Huang, A. De Luca, T. J. Atherton, M. Bird, C. Rosenblatt, and P. Carles, Phys. Rev. Lett. **99**, 204502 (2007).

[13] G. Pacitto, C. Flament, J.-C. Bacri, and M. Widom, Phys. Rev. E **62**, 7941 (2000).
[14] J. Ginder, *Encyclopedia of Applied Physics* (VCH Publishers, New York, 1996), Vol. 16, p. 487.
[15] A. Bombard, M. Knobel, M. R. Alcantara, and I. Joekes, J. Intell. Mater. Syst. Struct. **13**, 471 (2002).
[16] V. N. Goncharov, Phys. Rev. Lett. **88**, 134502 (2002).
[17] D. Oron, L. Arazi, D. Kartoon, A. Rikanati, U. Alon, and D. Shvarts, Phys. Plasmas **8**, 2883 (2001).
[18] P. Ramaprabhu, G. Dimonte, Y. N. Young, A. C. Calder, and B. Fryxell, Phys. Rev. E **74**, 066308 (2006).
[19] K. O. Mikaelian, Phys. Rev. E **78**, 015303(R) (2008).
[20] S.-I. Sohn, Phys. Rev. E **69**, 036703 (2004).
[21] Q. Zhang, Phys. Rev. Lett. **81**, 3391 (1998).